Subsonic cavity flow control with Micro-Magneto-Mechanical Systems (MMMS) microvalves

Thomas Arnoult, Colin Leclercq, Cécile Ghouila-Houri, A. Mazzamurro, R. Viard, Eric Garnier, C. Poussot-Vassal, A. Merlen, Denis Sipp, Philippe Pernod, et al.

Subsonic cavity flow control with Micro-Magneto-Mechanical Systems (MMMS) microvalves

T. Arnoult[a,*], C. Leclercq[b], C. Ghouila-Houri[a], A. Mazzamurro[a], R. Viard[c], E. Garnier[d], C. Poussot-Vassal[e], A. Merlen[a], D. Sipp[b], P.Pernod[a], A. Talbi[a]

[a] *Univ. Lille, CNRS, Centrale Lille, Univ. Polytechnique Hauts-de-France, UMR 8520 - IEMN - Institut d'Electronique de Microélectronique et de Nanotechnologie, F-59000 Lille, France France*

[b] *DAAA, ONERA The French Aerospace Lab, Meudon, F-92190, France*

[c] *JMH Conception Mulhouse F-68100 , France*

[d] *Univ. Lille, CNRS, ONERA, Arts et Metiers Institute of Technology, Centrale Lille, UMR 9014, Laboratoire de Mécanique des fluides de Lille—Kampé de Fériet, F-59000 Lille, France*

[e] *DTIS, ONERA The French Aerospace Lab, Université de Toulouse, F-31055 Toulouse, France*

Abstract

Flow control consists in modifying a flow natural state in order to converge towards another state which is considered as favorable, as drag or noise radiation might be reduced. In this paper, open-loop flow control experiments are carried out on a subsonic open-cavity flow. In the case of unstable flow control, the control focus is brought onto the flow fluctuations modifications rather than modification of the mean flow properties. Therefore, the forcing flexibility using arbitrary signals and the forcing linearity are essential for such flow control cases. In that sense, a linear array of Micro Magneto-Electro-Mechanical Systems actuators has been implemented to perform open-loop flow control experiments on an open-cavity. The actuators are able to generate both quasi-steady and pulsed jets with linear behavior. We proved the microvalves efficiency to damp the cavity oscillations. The quasi-steady jets reached a reduction of 20 dB in the cavity fundamental amplitude sound pressure level. Pulsed jets enabled an additional cavity tone amplitude reduction, which depends on the pulsating frequency and on the forcing amplitude. These results are a first step towards the implementation of the closed-loop control of the open-cavity flow.

Keywords: `MEMS actuators, Flow control, Open-cavity, Quasi-steady jets, Pulsed jets.`

*Corresponding author

Email address: `thomas.arnoult@centralelille.fr` (T. Arnoult)

1. Introduction

Flow control techniques can be defined as methods modifying a flow behavior in order to obtain positive changes in the flow [1]. On one hand, many applications have focused on the control of flow separation with unsteady fluidic actuators. In such a case, the forcing unsteadiness would not be sufficient on its own to modify the flow mean properties, which are meant to be controlled to change the flow state. The unsteady forcing must be combined with high mass flow rates to reach control efficiency. On the other hand, control of instabilities, such as the one developing in the subsonic flow over an open-cavity, control can be performed with lower mass flow rates, as the focus is brought onto the flow fluctuations modifications. Therefore, the forcing flexibility using arbitrary signals and the forcing linearity are essential for such flow control cases.

In this context, different technologies of actuators have been developed and employed in flow control applications. The following, non-exhaustive, state of the art sums up some of the widespread actuation technologies. Considering the review of Cattafesta and Sheplak [2] on actuators designed for active flow control applications, devices can be divided between moving surfaces actuators, plasma actuators and fluidic actuators. Regarding the first category, devices were developed for instance by Seifert *et al.* [3] or Sarno and Franke [4]. Seifert *et al.* performed flow separation control on an airfoil with piezoelectric unimorph actuators, while Sarno and Franke control the flow over an open-cavity with mechanical fences. The second category of actuators received great attention over the last decades. Plasma actuators in the form of single Dielectric Barrier Discharge (DBD) consists in two electrodes separated by a dielectric layer. The bottom electrode is connected to the ground, while the exposed one is supplied with an AC high voltage in the range of kV with a frequency in the range of kHz. The ambient air is ionized by the electrodes and an electrohydrodynamic force is induced, which can be used to pursue flow control objectives. For instance, Kurz *et al.* [5] performed boundary layer transition control experiments on an ONERA-D airfoil using DBD actuation. With a similar DBD actuator Maceda *et al.* [6] performed the stabilization of an open-cavity flow. The third category, reading fluidic actuators, can be decomposed into fluidic oscillators [7, 8], synthetic jets [9, 10, 11, 12] and pulsed jets [13, 14, 15, 16]. Fluidic oscillators were used for instance by Seele *et al.* [7, 8] in the form of sweeping jets benefiting from the coanda effect to perform flow separation control experiments on a wing of a Boeing-Bell V22. Synthetic jets are another common type of actuators alternating blowing and air sucking phases to add/subtract momentum into/from a flow. Mc Cormick [9] performed boundary layer separation control on an airfoil with directed synthetic jets. However, synthetic jets have a limited bandwith as their actuation frequency must be close to the actuator resonant frequency to induce flow momentum. Pulsed jet actuators circumvent this issue as their bandwith is larger, even though they require an external source of fluid. For instance, Bons *et al.* [13] studied the flow separation control on a low pressure turbine blade with pulsed jets used as vortex generators jets. All the previously presented actuators are macro-actuators, as they do not combine electrical and

mechanical micromachined components with characteristic dimensions between 1 mm and 1 μm [1]. Their integration on experimental setups might be limited by their power consumption, supply resources and size. These drawbacks vanish considering MEMS (Micro Electro Mechanical Systems) devices. MEMS actuators from the previously presented actuation categories have been developed. For instance, Kilberg *et al.* [17] designed a MEMS control surface for millimeter-scale rockets. Eijo *et al.* [18] built a pulsed micro-jet with DBD. Gimeno *et al.* [19] developed a synthetic jet relying on magneto-mechanical coupling, whose design has been enhanced by Gerbedoen *et al.* [20], who aimed at a wider bandwidth. Considering pulsed jets, Viard *et al.* [21] designed vertically assembled magneto-mechanical microvalves employed to perform flow separation control. Figure 1 synthesizes performances of some of the actuators described previously and performances of the actuators considered in the present study.

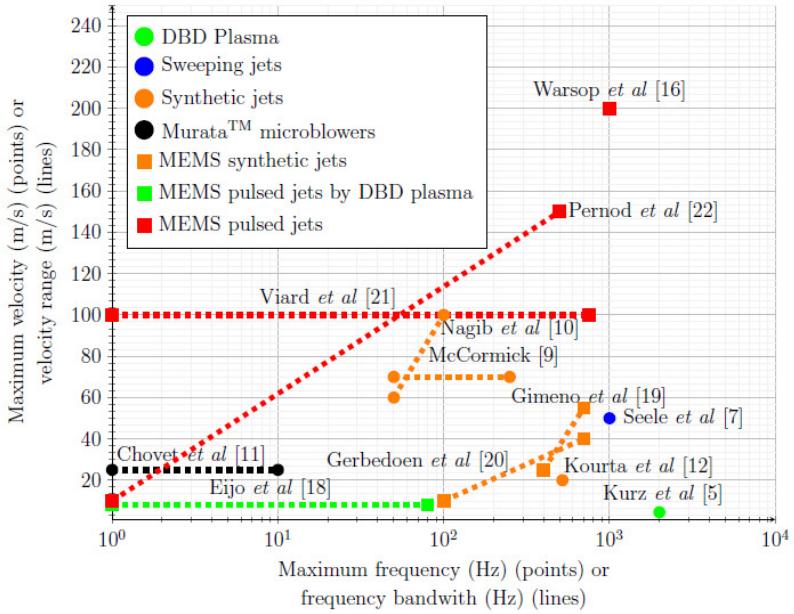

Figure 1: Comparison of fluidic actuators performances (inspired from [21]).

In the present study, Micro-Magneto-Mechanical Systems (MMMS) microvalves generating both quasi-steady and pulsed jets with a linear behavior are considered. The actuators, based on the technology presented in [22], have the advantage to be able to follow arbitrary command signal. A linear array of 15 microvalves has been integrated to an open cavity upstream edge to perform

open-loop flow control experiments. The open-cavity is a commonly studied geometry in fluid dynamics, with many practical applications. In the aeronautical domain, airplanes landing gear doors or weapon bays have cavity shapes [23]. These shapes can also be found on vehicles such as cars or trucks, considering wheel wells, trains between two carriages or even regarding telescope bays [24]. Flow over cavities have been extensively studied by Roshko [25], Rossiter [26] or East [27]. As depicted in Figure 2, the laminar or turbulent boundary layer developing upstream the cavity, characterized by a thickness δ and a momentum thickness θ, separates at the cavity upstream border. It results in a shear layer developing over the cavity of length L, depth D and span W. This shear layer undergoes hydrodynamic instabilities over the cavity, reattaches near the cavity downstream corner for deep open cavities characterized by an aspect ratio $L/D \leq 4$ according to Rossiter [26]. The vortices growing in the shear layer impact the trailing edge, generating acoustic waves which propagate upstream and excite the shear layer instabilities at the upstream corner. This flow description was proposed by Rossiter [26] and corresponds to an aeroacoustic feedback mechanism, for which oscillations are self-sustained. For deep cavities, this mechanism can be coupled with an acoustic resonance mechanism due to the cavity normal acoustic modes. This particular mechanism was investigated by East [27]. These phenomena can interact with each other, yielding a local maximum in the global modes growth rate. For low Mach numbers as in [27], the latter mechanism can be seen as enhancing the former mechanism response [28]. Both mechanisms result in the generation of flow-induced noise radiation and structural vibration, which may cause structural damage. We investigate in this paper the possibility of damping these flow oscillations through open-loop fluidic control, using our MMMS microvalves.

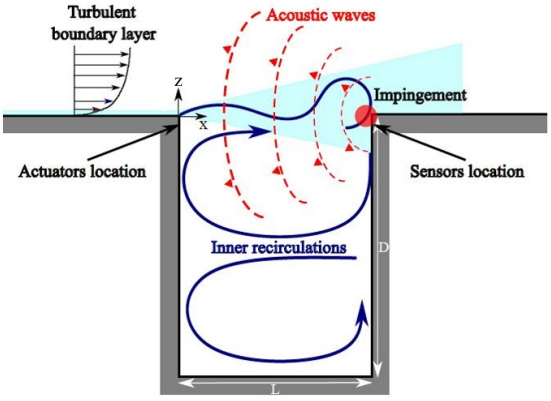

Figure 2: Illustration of the developing flow over an open-cavity with an upcoming turbulent boundary layer.

In this paper, the first part focuses on the microvalves design and fabrication process. The second part presents the MMMS actuators characterization performed with hot wire measurements. The third part describes the experimental setup in which an array of microvalves has been integrated and discusses the flow control results.

2. Device design and fabrication

2.1. Microvalve description and working principle

The normally open microvalve is composed of a 240 μm deep silicon micro-channel containing two inner walls and an outlet hole at one of its extremity. A 100 μm thick flexible Polydimethylsiloxane (PDMS) membrane surmounts this channel and is fixed to a 350 μm thick silicon pad. A couple of permanent NdFeB magnets of total thickness 2.5 mm is attached to the pad and is surrounded by a coil, contained in the microvalve packaging. This design, schematically presented in Figure 3, allows two different actuation types. To operate the microvalve, a source of pressurized air has to be supplied to the actuator, alongside with an electrical source, if pulsed jets are to be generated. The first actuation mode consists in generating a quasi-steady jet thanks to a pressure difference applied through the microvalve. Due to the pressure increase inside the micro-channel, the silicon pad and the magnets are lifted up to an equilibrium position. Hence, the air flows from the inlet to the submillimetric outlet. To generate a pulsed-jet, an electrical input signal is applied to the coil surrounding the magnets. Hence, the silicon pad oscillates around its equilibrium position defined by the inlet pressure. Therefore, the micro-channel height is modulated and a pulsed jet is generated at the microvalve outlet. The silicium pad considered here has an increased size compared to the one presented in [22]. This limits the apparition of non linearities in the actuation. Furthermore, the actuators have a large frequency bandwith and are not only used at their resonant frequency, which is an advantage regarding the control application of an open-cavity flow.

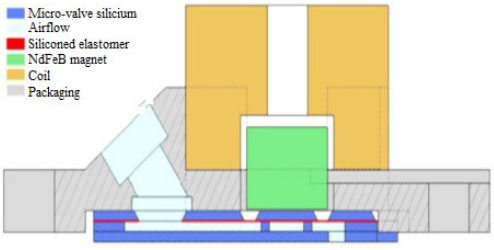

Figure 3: Schematic description of a MMMS microvalve.

2.2. Fabrication process

The fabrication process of the MMMS microvalves associates silicon micro-machining and rapid prototyping. Rapid prototyping was used to process the package of the microvalve that fixes the coil and allows the microvalve assembling. Silicon micro-machining techniques were exploited to realize both the membrane and the micro-channel parts. The membrane is processed (Figure 4 (a) and (b)) by first preparing and spin-coating a PDMS solution on a 350 μm thick wafer. After PDMS baking, the wafer is processed on its backside. Photo-lithography defines the silicon pad dimensions and Deep Reactive Ion Etching (DRIE) process is used to etch the silicon wafer. The process, called Bosch process, alternates a passivation phase using C_4F_8 and an etching phases using SF_6 gas to ensure anisotropic etching of silicon.

Thereby, the silicon wafer is etched over its thickness and the silicon pad is only maintained by the PDMS layer. This allows the pad to move and proceed to the actuation of the microvalve.

For the micro-channel part, two DRIE steps were needed (Figure 4 (c) and (d)) to manufacture the microfluidic channel and the output. This process is realized on a 500 μm thick double side polished silicon wafer. On one side, the micro fluidic channel is defined by photolithography. DRIE Bosch process etches the silicon by 250 μm which is the wanted depth for the microfluidic channel. Then, backside photo-lithography is needed to align the outlet with the front side microfluidic channel. The remaining 250 μm thick silicon is etched again using the Bosch process until the outlet is completely open.

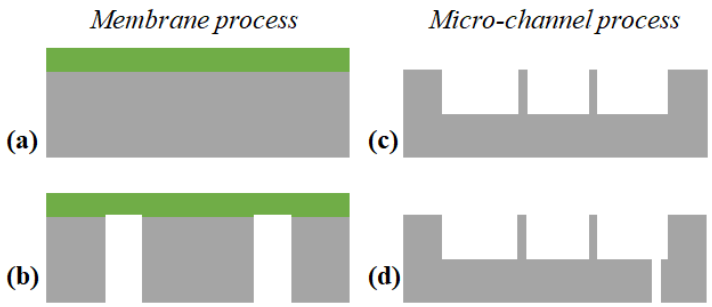

Figure 4: Fabrication process of the microvalve. Left: Membrane process with (a) PDMS spin-coating (b) Silicon pad etching. Right Micro-channel process: (c) frontside micro-channel etching (d) backside outlet etching

Figures 5 (a) and (b) are Scanning Electron Microscopy (SEM) pictures of the realized device parts. Figure 5 (a) shows the silicon pad etched over the wafer thickness and maintained by the PDMS layer. Figure 5 (b) shows one extremity of the microfluidic channel, where there is the outlet of the microvalve. This picture shows the two etching steps: the first up to half the wafer thickness for

the microfluidic channel and the second step opening the silicon wafer for the fluidic jet outlet.

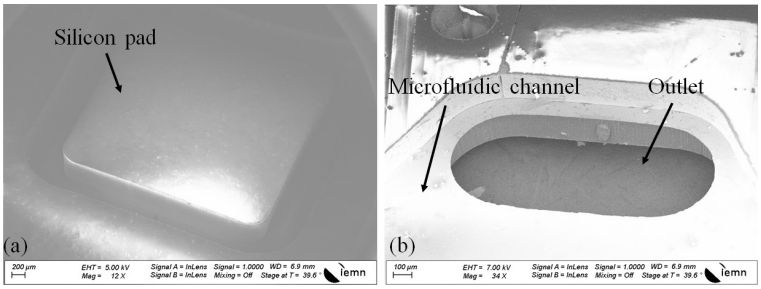

Figure 5: SEM (Scanning Electron Microscopy) pictures of the MMMS microvalve: (a) the membrane and the silicon pad (b) the extremity of the microfluidic channel with the outlet

2.3. Assembled microvalve

The microvalve outlet had to be adapted to the open-cavity geometry. To perform flow control experiments with the microvalves, their induced jets have to spread over the entire cavity span. Therefore, the submillimetric outlet was adapted towards a slot outlet. For a single microvalve, the slot length and height are respectively 12 mm and 0.2 mm. An example of assembled microvalve with the jet adapter is presented in Figure 6a. The adapters were fabricated by stereolithography in a Problack10 resin. It is composed of an upper and a lower part, which brought together induce a jet outlet angle of 45° as sketched in Figure 6b.

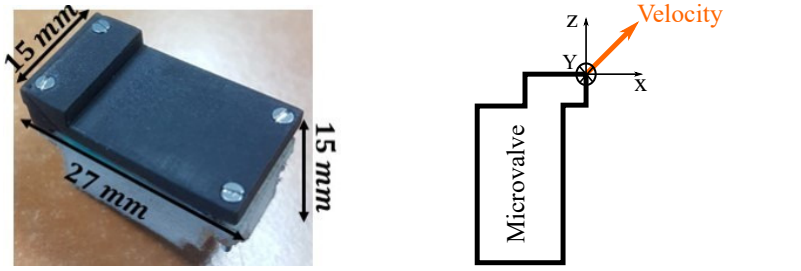

(a) Picture of an assembled microvalve.

(b) Scheme of a microvalve with associated axes.

Figure 6: Picture (6a) and scheme (6b) of a microvalve with associated axes.

3. Microvalves characterization

3.1. Characterization experimental setup

Once we assembled a set of 15 microvalves, we first individually characterized their quasi-steady jets and then their pulsed jets. microvalves were mounted as an array on a test bench as depicted in Figure 7. Hot wire measurements were performed to characterize the jets induced by the actuators. A Dantec 55P15 hot wire probe associated to a mini CTA 54T42 was used to perform measurements with a sampling frequency of 20 kHz over 1 s at each considered point.

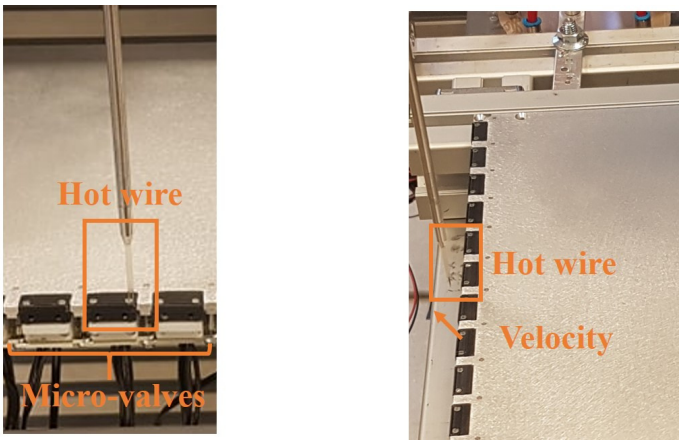

Figure 7: Test bench with the integrated microvalves array from two different views.

3.2. Quasi-steady jets characterization

Each actuator was supplied with a pressure difference, set up with respect to the ambient pressure, varied between 0 and 200 mbar. The induced flow rate through the microvalves was measured and proved that the mounted microvalves have the same flow rate/pressure difference characteristics. For pressure differences lower than 25 mbar no flow rate could be measured. However, for pressure differences higher than 25 mbar the flow rate/pressure difference relation is affine as described by the following equation:

$$\mathrm{D} = -0.15 + 0.01\Delta\mathrm{P} \text{ with D is L/min and } \Delta\mathrm{P} \text{ in mbar.} \quad (1)$$

Figure 8 shows for a tens of microvalves the flow rate against pressure curves, along with the mean flow rate/pressure characteristic. In this chart, the scattering between the highest and the lowest flow rates measured for a driving

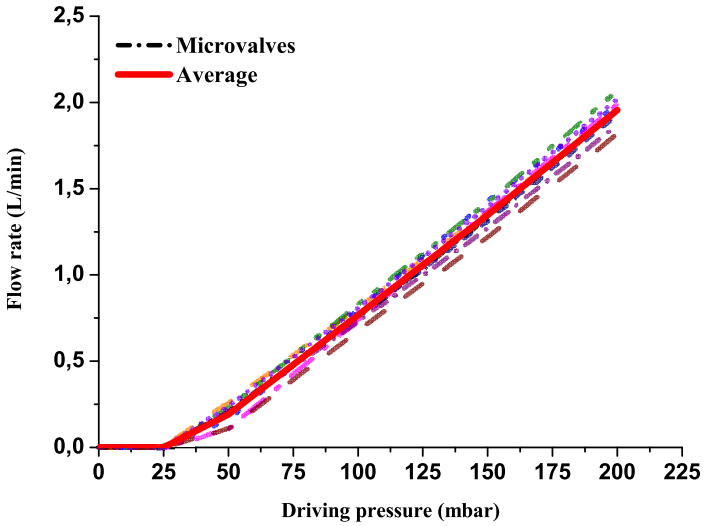

Figure 8: Microvalves flow rate/pressure characteristics.

pressure above 100 mbar is about 14 %. This scattering can be explained by the manual assembly of each layer composing the microvalves.

To further characterize the quasi-steady jet of a microvalve, hot wire measurements in the (YZ) and (XZ) planes were carried out. For these measurements, the flow crosses the measurement plane with a 45° angle in the (XZ) plane. The hot wire probe is placed parallel to the Y axis. Therefore, the velocity measured by the hot wire is a combination of the velocity X and Z components. One microvalve was supplied with a pressure difference of $\Delta P = 150$ mbar, yielding a flow rate D of 1.5 L/min. Figures 9 and 10 respectively present the measurements in the (YZ) and (XZ) planes. For these measurements, the axes origin is taken at the microvalve outlet center. As sketched in Figure 6b, X, Y and Z axes are defined with respect to the actuators outlet.
As depicted in Figure 9, it was observed that the jet outlet is centered on the slot exit. The maximum velocity reached for $\Delta P = 150$ mbar is about 25 m/s. Figure 10 presents the jet velocity mapping for the same parameters in the (XZ) plane. The jet outlet angle of 45 ° can be measured from this mapping.

3.3. Pulsed jets characterization

Afterwards, we characterized the microvalves' pulsed jets. The entire array was supplied with a total pressure difference of 250 mbar. One microvalve at a time was supplied with an electrical signal. Input signals used were sine

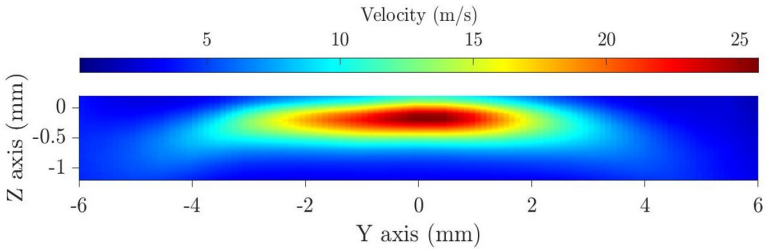

Figure 9: Quasi-steady jet mapping in the (YZ) plane for $\Delta P = 150$ mbar.

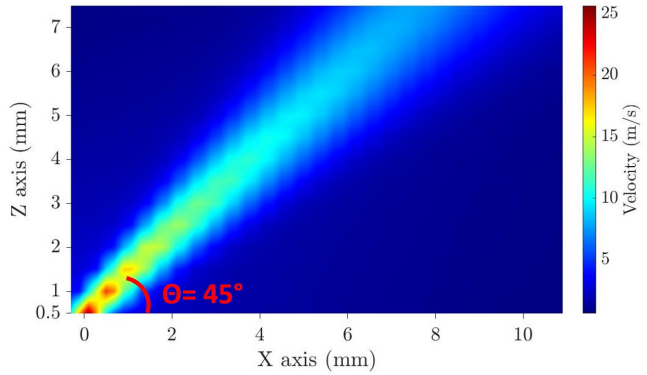

Figure 10: Quasi-steady jet mapping in the (XZ) plane for $\Delta P = 150$ mbar.

waves of the form $A\sin(2\pi ft)$ with amplitude values A of 0.5 V, 1 V, 1.5 V and 2 V and frequencies f ranging from 20 Hz up to 380 Hz. The amplitude denoted A corresponds to the signal generator amplitude, which is firstly fed to a linear amplifier before it reaches the actuators. Hot wire measurements were performed at the microvalve maximum velocity location for $X = 0.5$ mm. Figure 11 illustrates the input signal used to control the pulsed jet and the actuator outlet velocity post processing performed on the measurements for several actuation cases. Considering an input signal of frequency 240 Hz and amplitude 2V in Figure 11a, the associated velocity measurements is presented in Figure 11b. It can be observed that the velocity oscillates around a mean value of 22 m/s. Figure 11c presents the raw velocity Power Spectral Density (PSD). It is composed of three peaks: one at 240 Hz corresponding to the fundamental frequency of the actuation and two others respectively at 480 Hz and 720 Hz corresponding to harmonics. Harmonics are largely dominated by the fundamental frequency, as their PSD is lower by at least 10 dB. In Figure 11d, we therefore consider the output signal filtered at the sinusoidal forcing frequency and four amplitudes A. The velocity modulation depth appears to

evolve linearly with A.

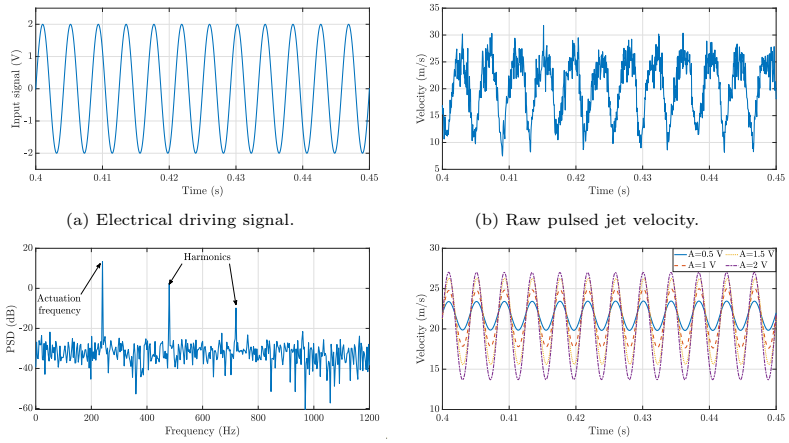

(a) Electrical driving signal.

(b) Raw pulsed jet velocity.

(c) Microvalve velocity spectrum.

(d) Filtered pulsed jet velocity.

Figure 11: Actuator input signal (11a), velocity measurement (11b), spectrum (11c) and comparison of the filtered velocity around the actuation frequency for different amplitudes (11d), f = 240 Hz and A = 0.5 V, 1 V, 1.5 V and 2 V.

The microvalves transfer function, defined as the ratio between the velocity hot wire measurements and the signal generator driving signal, have then been computed. The transfer function Bode diagram of one microvalve is presented in Figure 12.

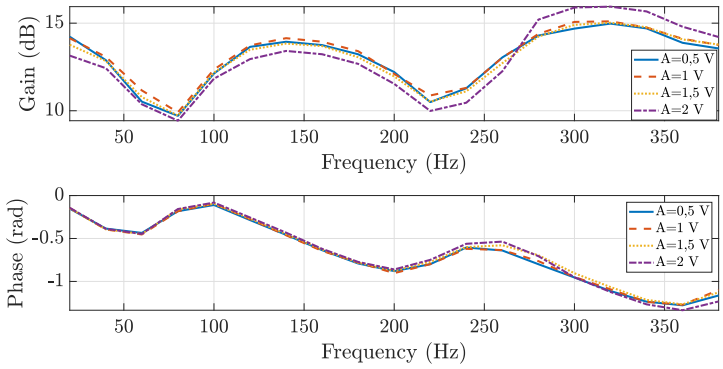

Figure 12: Microvalve transfer function Bode diagrams.

The gain plot indicates that the actuator behaves linearly as the four curves

for the different amplitudes superimpose, except for A = 2 V and f ≥ 250 Hz. Considering the phase plot for a given frequency, whatever the input signal amplitude is, the same delay between the signal command and the outlet velocity is induced. Figure 13 further proves the linear behavior of the microvalves. An input signal composed of two sine waves respectively with frequencies of 100 Hz and 200 Hz and with the same amplitudes was used. The microvalve response was measured with a hot wire. Both the input and output signals PSD are presented in Figure 13. The input signal PSD is obviously composed of two peaks respectively at 100 Hz and 200 Hz with the same amplitude. The output signal PSD is also composed of two peaks at these frequencies pointing out the superposition principle respected by the actuator. The amplitude difference between the two peaks is explained by the transfer function presented previously which does not exhibit a flat gain curve.

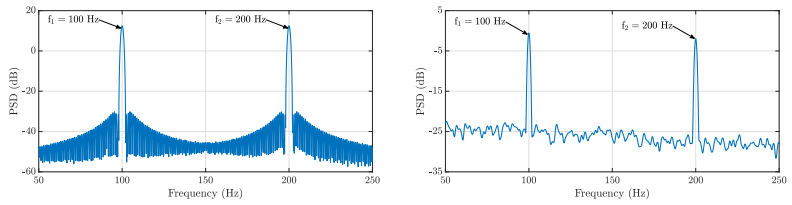

(a) Input signal PSD.

(b) Hot wire measurement PSD.

Figure 13: Illustration of the actuator superposition principle.

The linear behavior of such actuators implies their ability to be controlled with arbitrary signals and constitutes a first step towards future works which will be focused on the implementation of closed-loop control strategies of the flow over the open-cavity.

4. Flow control experiments

4.1. Experimental setup

After their characterization, MMMS actuators were used for open-loop flow control experiments carried out in the S19 wind tunnel at ONERA Meudon. In the present study, the objective is to integrate a linear array of 15 microvalves such that their jet can interact with the shear layer developing over the cavity. Therefore, it was decided to integrate the microvalves on the upstream cavity corner, as depicted in Figure 14b. As detailed in [29], the shear layer instabilities are sensitive to forcings close to the cavity upstream edge. The actuators are located just below the shear layer at the cavity upstream edge, and out-coming jets interact with the shear layer due to their angle of 45° with respect to the shear layer.

The wind tunnel consists of a plenum chamber, a rectangular test section of length 1910 mm, span 300 mm and height 150 mm, followed by a diverging duct.

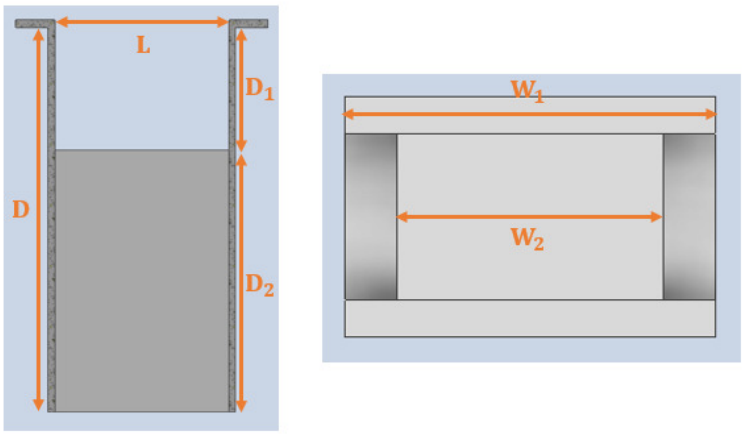

(a) Sketch of the cavity geometry with depths and spans of the two cavity parts.

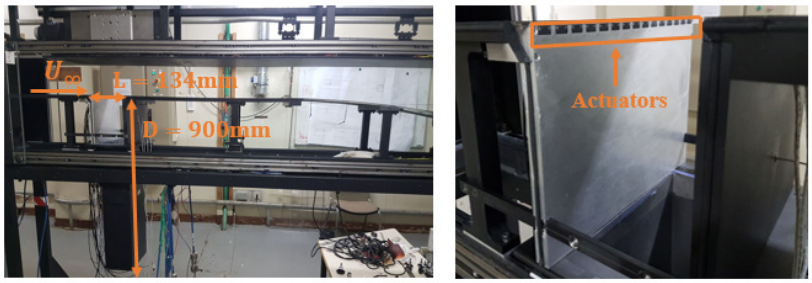

(b) Pictures of the wind tunnel experimental setup with the cavity dimensions (left) and integration of the actuator array (right).

Figure 14: Sketch of the cavity with the dimensions (14a) and photography of the experimental setup inside the wind tunnel (14b).

The flow developing in the test section is turbulent due to a carborundum strip placed upstream the cavity. The cavity of length L = 134 mm is inserted on the lower wall of the rectangular test section. The cavity is composed of two parts with different spans W_1 and W_2. The first part of depth $D_1 = 300$ mm spans over $W_1 = 300$ mm. Below, the second part of depth $D_2 = 600$ mm spans over $W_2 = 216$ mm. Therefore, the cavity total depth D equals 900 mm. A sketch of the cavity with the dimensions is presented in Figure 14a. The second part of the cavity was added such that the open-cavity flow oscillation frequencies matched the actuators bandwith. Stagnation pressure P_i and total temperature T_i measurements are performed in the wind tunnel plenum chamber. 17 static pressure probes are located along the upper wall of the test section and divergent

duct. To characterize the cavity flow dynamics, 4 Kulite unsteady pressure sensors XCQ-093-15A (15PSI) are integrated to the cavity downstream wall, 3 mm below the edge. These sensors have a resonant frequency of 200 kHz and a sensitivity of 1 μV/Pa, according to the manufacturer. The Kulite sensors output are passed through an amplifier of gain 50. Data are acquired using a National Instruments chassis with 18-bits PXI-6284 module characterized by a 500 kHz bandwidth. The acquisition chain enables simultaneous recordings of P_i, T_i, the ambient pressure P_{atm}, the flow velocity U_∞ (deduced from pressure measurements using a Pitot tube upstream the cavity), the 4 unsteady pressure measurements from the Kulite sensors and the actuator input signal. With a turbulence intensity of $\frac{u'}{U}$, of 0.3 %, where u' is the root-mean-square of the turbulent velocity fluctuations and $\bar{U}$ the mean velocity, the S19 wind-tunnel is a quiet wind tunnel.

4.2. Unforced flow dynamics characterization

First measurements were dedicated to the flow dynamics characterization without microvalves jets. The aim is to find a flow regime with low frequency oscillations. Velocities U_∞ ranging from 10 m/s to 46 m/s were explored. The Sound Pressure Level (SPL), expressed in dB, obtained from the Power Spectral Density (PSD) of each Kulite sensors were computed based on the following relationship:

$$\mathrm{SPL} = 20 \log_{10} \left(\frac{\sqrt{\mathrm{PSD}}}{P_{ref}} \right), \tag{2}$$

where $P_{ref} = 20$ μPa is a reference pressure corresponding to the threshold of human hearing. Depending on the freestream velocity U_∞, periodic or quasi-periodic flow regimes were identified. From pressure measurements, three periodic oscillating flow regimes were identified respectively for freestream velocities of $U_\infty = 20$ m/s, $U_\infty = 30$ m/s and $U_\infty = 34$ m/s. Resonant frequencies for these three freestream velocities are presented in Table 1.

Velocity U_∞ (m/s)	Resonant frequency (Hz)			
20	128.6	257.2	385.9	
30	122	244	366	
34	124	247	371	495

Table 1: Resonant frequencies for three values of the freestream velocity U_∞.

The pressure spectrum for $U_\infty = 20$ m/s is presented in Figure 15. It is composed of a parasitic peak at 50 Hz due to electrical noise and three peaks characterizing the flow dynamics. The flow spectrum is therefore composed of a fundamental oscillation frequency f_1 at 128.6 Hz and two harmonics f_2 and f_3

respectively at 257.2 Hz and 385.9 Hz. Signals were acquired over a duration of 45 s with a sampling frequency $f_s = 10$ kHz. The signal PSD was then computed with a Welch's algorithm based on 60 Hamming windows and an overlap of 50%, yielding a frequency resolution of 0.11 Hz. The 4 Kulite sensors indicate the same oscillation frequencies and similar values of SPL within a couple of dB. The results presented in this section are based on one of the 4 unsteady pressure sensors.

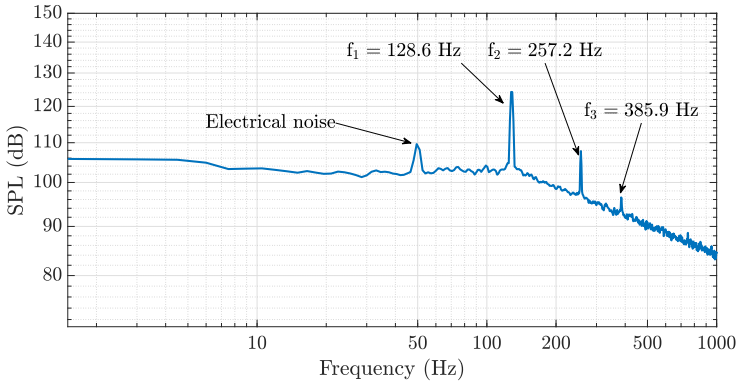

Figure 15: SPL (dB) flow spectrum near the downstream edge of the cavity for $U_\infty = 20$ m/s.

4.3. Quasi-steady jets

For each of the three freestream velocities, effects of quasi-steady jets on the flow dynamics were studied. Actuators driving pressures are presented in Table 2.

ΔP (mbar)							
0	150	175	200	225	250	275	290

Table 2: Actuators driving pressure.

Quasi-steady jets reduced the amplitudes of the peaks at the resonant frequencies. Their effects for a freestream velocity of 20 m/s can be observed in Figure 16. The fundamental frequency is reduced by 20.4 dB and the harmonic peaks completely vanish for a driving pressure above 250 mbar. From these spectra and for the different freestream velocities, the decrease in amplitude of the cavity fundamental frequency peak was computed. Figure 17 shows the effect of the quasi-steady jets on the cavity fundamental SPL. The

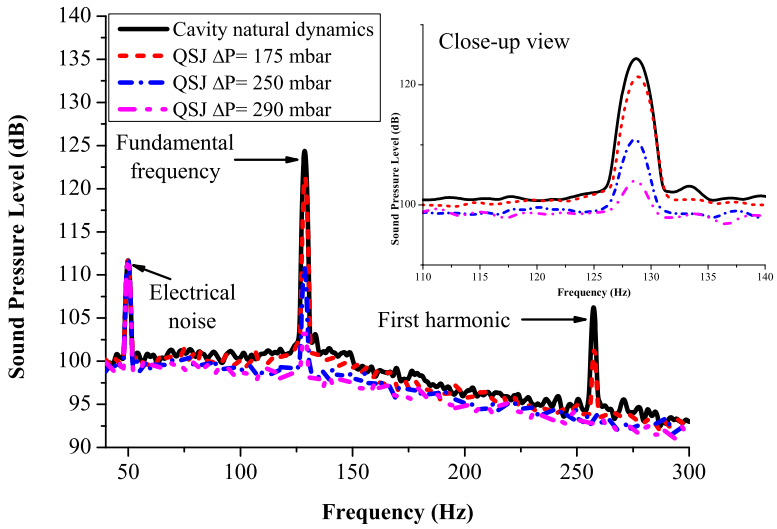

Figure 16: Flow spectra for $U_\infty = 20$ m/s and different driving pressure generating quasi-steady jets.

quasi-steady jets reduce the fundamental frequency amplitude by 20.4 dB for $\Delta P = 290$ mbar and $U_\infty = 20$ m/s. The amplitude reduction observed can be explained by the interaction of jets with the shear layer developing over the cavity. The 45° inclined jets might deflect the shear layer to the top, mitigating its interaction with the downstream corner. Effects of the quasi-steady jets on the cavity fundamental frequency is dependent on both the microvalves driving pressure ΔP and on the freestream velocity U_∞. For a fixed value of U_∞, the higher ΔP is, the more effect quasi-steady jets have on the cavity fundamental resonant frequency. In addition, for a fixed value of ΔP, the higher the freestream velocity U_∞ is, the less effect microvalves have on the cavity resonant frequency. As experiments at several values of freestream velocities U_∞ are performed at constant values of ΔP, effects of the quasi-steady steady jets on the fundamental resonant frequency is less important when U_∞ is increased. For $U_\infty = 30$ m/s, the amplitude reduction is only of 12.6 dB for the same ΔP of 290 mbar. For $U_\infty = 34$ m/s, the quasi-steady jets have no effect on the flow dynamics, regardless of the imposed driving pressure. Measurements performed at these three velocities show the actuators authority limit on the flow dynamics.

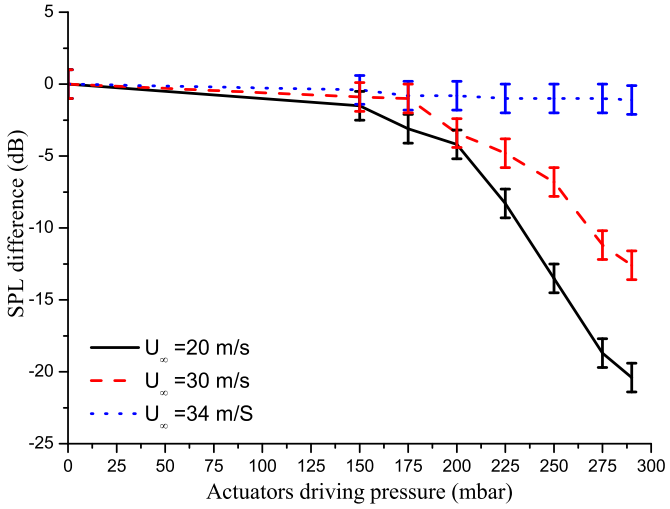

Figure 17: Evolution of the fundamental frequency SPL (dB) against the actuators driving pressure for different velocities.

4.4. Evaluation of microvalves control efficiency

In order to compare results obtained with the quasi-steady jets to those obtained in passed similar studies, the blowing coefficient B_c, firstly proposed by Vakili and Gauthier [30] for rectangular cavities has been calculated. This coefficient is defined as the mass flow rate of the actuator normalized by a typical mass flow rate of the cavity, where ρ_∞ denotes the freestream density and $A_{cavity} = LW$:

$$B_c = \frac{\dot{m_{inj}}}{\rho_\infty U_\infty A_{cavity}}. \tag{3}$$

The results obtained for $U_\infty = 20$ m/s and $\Delta P = 290$ mbar are compared in Figure 18 to results from different open-loop control studies of a cavity flow. This chart presents the distribution of B_c in % against the SPL reduction in dB.

Depending on the study-cases and the actuators technology used, different SPL reduction in the cavity oscillation were obtained. In the present study, measurements were realized on an open-cavity of aspect ratio $L/D = 0.15$ and for Mach numbers M varying between 0.06 and 0.1. The control was performed

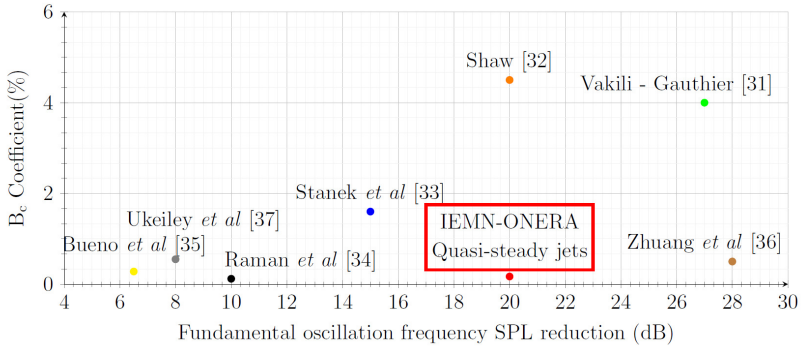

Figure 18: Evolution of the B_c coefficient against the fundamental resonant frequency SPL (dB) reduction for different studies and actuation technologies.

with MMMS microvalves and the SPL reduction obtained with the quasi-steady jets is compared with other studies. Studies presented in Figure 18 were performed on different study cases and different Mach numbers implying different flow dynamics. Shaw [31] considered an open-cavity such that $L/D = 6.5$ with M ranging from 0.6 up to 1.05. The control was performed with pulsed jets integrated to the upstream cavity border. The study case presented by Vakili and Gauthier [30] was such that $M = 1.8$ and for a cavity characterized by $L/D = 2.54$. Momentum was added to the flow through perforated plates placed upstream the cavity. This results in modified boundary layer properties affecting the cavity oscillations amplitudes. Stanek *et al.* [32] used 4 high frequency fluidic actuators to control the flow over a cavity of aspect ratio $L/D = 5$ with M varying between 0.4 and 1.35. Raman and Raghu [33] studied a cavity of length to depth ratio of 6 with Mach flows ranging between 0.4 and 0.7. They performed control experiments with sweeping jets benefiting from the coanda effect placed on the bottom floor of the cavity near the upstream and downstream edges. Bueno *et al.* [34] focused on a cavity for which L/D was varied between 5 and 9 with a freestream Mach number of 2. Their actuators were commercialized high speed valves (General Valve Series 9) pressurized up to 11 bar. Due to the actuators size, a staggered configuration was employed to integrate the valves to the experimental setup. Zhuang *et al.* [35] studied a cavity of length to depth ratio of 5.16 with a flow Mach number of 2. The actuators employed simply consist of micro-holes of 400 μm diameter supplied with a pressurized source of nitrogen. On their side, Ukeiley *et al.* [36] considered a cavity of length to depth ratio of 5.6 or 9 with Mach numbers of 0.6 and 0.75 and the control was performed with powered whistles. In Figure 18, low B_c coefficients correspond to low energy consumption control systems, while efficient controllers are represented on this chart with a high SPL reduction value. Therefore, it can be observed that the microvalves provide a satisfying compromise between

efficiency and energy cost compared to the other studies.

4.5. Pulsed jets

We then tested the effect of pulsed jets. Pulsed jets modulate the velocity about a mean value fixed by the driving pressure ΔP, we therefore expect at least the same amplitude reduction at the fundamental frequency. In Figure 19, cavity spectra for $U_\infty = 20$ m/s are compared for quasi-steady jets and pulsed jets with a driving pressure of $\Delta P = 250$ mbar. The unsteady forcing highlighted in this Figure is characterized by a pulsating frequency of 140 Hz and two different input signal amplitudes of 1 V and 2 V. Two phenomena can be observed. Firstly, a peak at the pulsating frequency appears in the spectrum, which SPL depends on the forcing amplitude and on the actuation frequency. For a frequency of 140 Hz and an amplitude of A = 1 V, the SPL reaches 103 dB, while for A = 2 V the SPL reaches 108 dB, yielding a difference of 5 dB between the two pulsating cases. Secondly, a further reduction in the cavity fundamental frequency amplitude of 3 to 5 dB, depending on the frequency and forcing amplitude, is observed due to the pulsed jets. These measurements were performed for the sets of parameters described in Table 3. These two phenomena indicate a non-linear response of the cavity to the unsteady forcing as a forcing at a different pulsating frequency induces an effect on the cavity fundamental frequency amplitude. However, the cavity response at the forcing frequency is quasi-linear which is an important result for setting up closed-loop control strategies in future work.

ΔP (mbar)	200, 250 290
Frequencies (Hz)	80 to 300 (step of 20 Hz)
Amplitudes (V)	0.5 V, 1 V, 1.5 V2 V

Table 3: Sets of parameters used for the study of pulsed jets effects.

5. Conclusion

This paper presented the characterization of MMMS microvalves, their integration on an open-cavity in a wind tunnel and their use in open-loop flow control experiments. The actuators command flexibility and linearity make them interesting for the control of flows such as the one developing over an open-cavity, as the microvalves act on the flow unsteadiness with the generated forcing fluctuations. Thanks to the microvalves small size, a linear array of 15 actuators was successfully integrated and flush mounted in a wind tunnel to perform flow control experiments on an open-cavity. The quasi-steady jets induced by the MEMS actuators reduced the cavity tones amplitude down to 20.4 dB for a freestream velocity of 20 m/s. Compared to quasi-steady jets and depending on the actuation frequency and the amplitude, pulsed jets reduced further the cavity tones down by 5 dB. Furthermore, the pulsed jets frequency

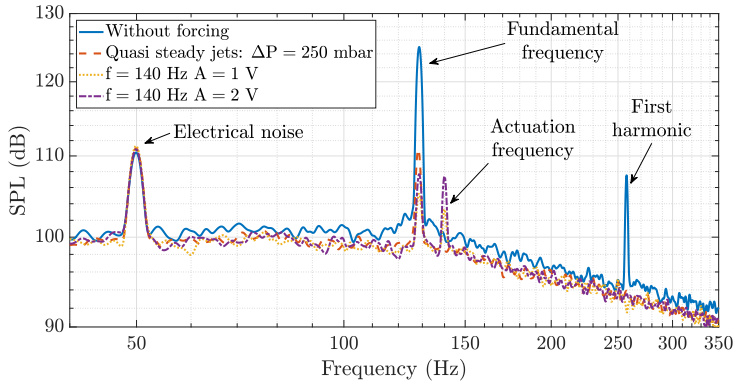

Figure 19: SPL (dB) spectra comparison with $U_\infty = 20$ m/s for a quasi-steady jets case and two different pulsed jets cases.

appears in the cavity spectrum depending on the input voltage amplitude. This significant result is of interest for future works dedicated to the closed loop-control of the flow over the open-cavity. The closed-loop strategy would benefit from these actuators as the microvalves are able to follow an arbitrary command signal delivered by the controller. The actuators command flexibility would be an advantage in implementing the closed-loop control of the open-cavity flow. Furthermore, the effect of quasi-steady jets will be limited as closed-loop experiments will be carried out with low driving pressures. Therefore, the effects of the closed-loop control would be only due to the unsteady part of the jets. The aim of the closed-loop control strategy will be to further reduce the actuators energy consumption and further damp the cavity resonance SPL.

6. Acknowledgments

This work was funded by the French National Research Agency (ANR) in the framework of the ANR ASTRID MATURATION "CAMELOTT-MATVAL" Project. It is supported by the regional platform CONTRAERO, the CPER ELSAT 2020 Project and the CPER RITMEA 2021-2027 Project. The Innovation Defense Agency (AID) has also financially sustained this work. The authors also thank RENATECH, the French national nanofabrication network, and FEDER.

7. References

References

[1] M. Gad-el Hak, Flow control: passive, active, and reactive flow management, Cambridge University Press, Cambridge, 2000.

[2] L. N. Cattafesta, M. Sheplak, Actuators for Active Flow Control, Annual Review of Fluid Mechanics 43 (1) (2011) 247–272.

[3] A. Seifert, S. Eliahu, D. Greenblatt, I. Wygnanski, Use of Piezoelectric Actuators for Airfoil Separation Control, AIAA JOURNAL 36 (8) (1998) 4.

[4] R. L. Sarno, M. E. Franke, Suppression of flow-induced pressure oscillations in cavities, Journal of Aircraft 31 (1) (1994) 90–96.

[5] A. Kurz, S. Grundmann, C. Tropea, M. Forte, A. Seraudie, O. Vermeersch, D. Arnal, R. Goldin, R. King, Boundary Layer Transition Control using DBD Plasma Actuators, Aerospace Lab Journal (2013) 9.

[6] G. Y. C. Maceda, E. Varon, F. Lusseyran, B. R. Noack, Stabilization of a multi-frequency open cavity flow with gradient-enriched machine learning control, arXiv:2202.01686 [physics].

[7] R. Seele, P. Tewes, R. Woszidlo, M. A. McVeigh, N. J. Lucas, I. J. Wygnanski, Discrete Sweeping Jets as Tools for Improving the Performance of the V-22, Journal of Aircraft 46 (6) (2009) 2098–2106.

[8] E. A. Whalen, D. S. Lacy, J. C. Lin, M. Y. Andino, A. E. Washburn, E. C. Graff, I. J. Wygnanski, Performance Enhancement of a Full-Scale Vertical Tail Model Equipped with Active Flow Control, in: 53rd AIAA Aerospace Sciences Meeting, American Institute of Aeronautics and Astronautics, Kissimmee, Florida, 2015.

[9] D. McCormick, Boundary layer separation control with directed synthetic jets, in: 38th Aerospace Sciences Meeting and Exhibit, American Institute of Aeronautics and Astronautics, Reno,NV,U.S.A., 2000.

[10] H. Nagib, J. Kiedaisch, I. J. Wygnanski, A. Stalker, T. Wood, M. McVeigh, First-In-Flight Full-Scale Application of Active Flow Control: The XV-15 Tiltrotor Download Reduction, NATO Report.

[11] C. Chovet, M. Lippert, L. Keirsbulck, J.-M. Foucaut, Dynamic characterization of piezoelectric micro-blowers for separation flow control, Sensors and Actuators A: Physical 249 (2016) 122–130.

[12] A. Kourta, C. Leclerc, Characterization of synthetic jet actuation with application to Ahmed body wake, Sensors and Actuators A: Physical 192 (2013) 13–26.

[13] J. P. Bons, R. Sondergaard, R. B. Rivir, The Fluid Dynamics of LPT Blade Separation Control Using Pulsed Jets, Journal of Turbomachinery 124 (1) (2002) 77–85.

[14] H. Lou, F. S. Alvi, C. Shih, Active and Adaptive Control of Supersonic Impinging Jets, AIAA Journal 44 (1) (2006) 58–66.

[15] F. S. Alvi, C. Shih, R. Elavarasan, G. Garg, A. Krothapalli, Control of Supersonic Impinging Jet Flows Using Supersonic Microjets, AIAA Journal 41 (7) (2003) 1347–1355.

[16] C. Warsop, M. Hucker, A. J. Press, P. Dawson, Pulsed Air-jet Actuators for Flow Separation Control, Flow, Turbulence and Combustion 78 (3-4) (2007) 255–281.

[17] B. G. Kilberg, D. S. Contreras, J. Greenspun, K. S. J. Pister, MEMS aerodynamic control surfaces for millimeter-scale rockets, in: 2017 International Conference on Manipulation, Automation and Robotics at Small Scales (MARSS), IEEE, Montreal, QC, 2017, pp. 1–5.

[18] P. G. Eijo, R. Sosa, J.-L. Aider, J. M. Cabaleiro, Control of air microjets by the use of dielectric barrier discharges, Sensors and Actuators A: Physical 305 (2020) 111937.

[19] L. Gimeno, A. Talbi, R. Viard, A. Merlen, P. Pernod, V. Preobrazhensky, Synthetic jets based on micro magneto mechanical systems for aerodynamic flow control, Journal of Micromechanics and Microengineering 20 (7) (2010) 075004.

[20] J.-C. Gerbedoen, A. Talbi, R. Viard, V. Preobrazhensky, A. Merlen, P. Pernod, Joint International Laboratory LIA LICS, Elaboration of Compact Synthetic Micro-jets Based on Micro Magneto-mechanical Systems for Aerodynamic Flow Control, Procedia Engineering 120 (2015) 740–743.

[21] R. Viard, A. Talbi, C. Ghouila-Houri, A. Kourta, A. Merlen, P. Pernod, Magneto-mechanical micro-valve for active flow control, Sensors and Actuators A: Physical 316 (2020) 112387.

[22] P. Pernod, V. Preobrazhensky, A. Merlen, O. Ducloux, A. Talbi, L. Gimeno, R. Viard, N. Tiercelin, MEMS magneto-mechanical microvalves (MMMS) for aerodynamic active flow control, Journal of Magnetism and Magnetic Materials 322 (9-12) (2010) 1642–1646.

[23] C. W. Rowley, D. R. Williams, Dynamics and control of high-reynolds-number flow over open cavities, Annual Review of Fluid Mechanics 38 (1) (2006) 251–276.

[24] L. N. Cattafesta, Q. Song, D. R. Williams, C. W. Rowley, F. S. Alvi, Active control of flow-induced cavity oscillations, Progress in Aerospace Sciences 44 (7-8) (2008) 479–502.

[25] A. Roshko, Some Measurements of Flow in a Rectangular Cutout, Tech. rep., National Advisory Committee for Aeronautics (1955).

[26] J. E. Rossiter, Wind tunnel experiments on the flow over rectangular cavities at subsonic and transonic speeds, RAE Technical Report No. 64037.

[27] L. East, Aerodynamically induced resonance in rectangular cavities, Journal of Sound and Vibration 3 (3) (1966) 277–287.

[28] S. Yamouni, D. Sipp, L. Jacquin, Interaction between feedback aeroacoustic and acoustic resonance mechanisms in a cavity flow: a global stability analysis, Journal of Fluid Mechanics 717 (2013) 134–165.

[29] D. Sipp, P. J. Schmid, Linear Closed-Loop Control of Fluid Instabilities and Noise-Induced Perturbations: A Review of Approaches and Tools1, Applied Mechanics Reviews 68 (2) (2016) 020801.

[30] A. D. Vakili, C. Gauthier, Control of cavity flow by upstream mass-injection, Journal of Aircraft 31 (1) (1994) 169–174.

[31] L. Shaw, Active control for cavity acoustics, in: 4th AIAA/CEAS Aeroacoustics Conference, American Institute of Aeronautics and Astronautics, Toulouse,France, 1998.

[32] M. Stanek, G. Raman, V. Kibens, J. Ross, J. Odedra, J. Peto, Control of cavity resonance through very high frequency forcing, in: 6th Aeroacoustics Conference and Exhibit, American Institute of Aeronautics and Astronautics, 2000.

[33] G. Raman, S. Raghu, Cavity Resonance Suppression Using Miniature Fluidic Oscillators, AIAA Journal 42 (12) (2004) 2608–2612.

[34] P. Bueno, O. Unalmis, N. Clemens, D. Dolling, The effects of upstream mass injection on a Mach 2 cavity flow, in: 40th AIAA Aerospace Sciences Meeting & Exhibit, American Institute of Aeronautics and Astronautics, 2002.

[35] N. Zhuang, F. Alvi, C. Shih, Another Look at Supersonic Cavity Flows and Their Control, in: 11th AIAA/CEAS Aeroacoustics Conference, American Institute of Aeronautics and Astronautics, Monterey, California, 2005.

[36] L. Ukeiley, M. Sheehan, F. Coiffet, F. Alvi, S. Arunajatesan, B. Jansen, Control of Pressure Loads in Geometrically Complex Cavities, Journal of Aircraft 45 (3) (2008) 1014–1024.

Highlights

- A design of Micro-Magneto_Mechanical Systems (MMMS) microvalves for flow control is presented
- The fabrication process based on micro-machining techniques is described
- Hot wire characterizations highlight the microvalves linear behavior
- A linear array of microvalves is integrated on an open-cavity in a wind tunnel
- Open-loop flow control experiments are performed and discussed

Author biography

Thomas Arnoult received the Engineering Degree from ISAE-ENSMA (Institut SUpérieur de l'Aéronautique et de l'Espace-Ecole Nationale Supérieure de Mécanique et d'Aérotechnique) and a Degree of Master of Science in Aerospace Dynamics from the Cranfield University (United Kingdom). After graduation in December 2019, he started a PhD at the IEMN, UMR CNRS 8520 Institute, in partnership with the ONERA, the French Aerospace Lab, regarding the use of innovative micro-actuators and micro-sensors in active flow control strategies.

Colin Leclercq has been a research engineer at the Department of Aerodynamics, Aeroelasticity, Acoustics (DAAA) of ONERA since 2018, specializing in closed-loop flow control. He obtained his PhD in fluid mechanics from LMFA, Ecole Centrale de Lyon in 2013 and held postdoctoral positions at the Department of Mathematics in the University of Bristol (2014-2016) and at ONERA DAAA (2016-2018).

Cécile Ghouila-Houri received her MS degree in Engineering with specialization in Micro-Nanotechnology, Wave Physics and Telecommunications from Ecole Centrale de Lille in 2015 and began her PhD in November 2015, joining the ONERA, the French Aerospace Lab, and the IEMN, the Institute of Electronics, Microelectronics and Nanotechnology of Lille. After graduation in October 2018, she joined Centrale Lille as Associate Professor in September 2019 and IEMN UMR CNRS 8520 as researcher. Her research concerns the development of microsystems (micro-sensors and micro-actuators) for fluids dynamics and aeronautics applications.

Aurélien Mazzamurro received his MS degree in Engineering with specialization in Micro-Nanotechnology, Wave Physics and Telecommunications from Centrale Lille in 2017 and began his PhD in November 2017 on SAW based magnetoelastic sensors, joining the IEMN, the Institute of Electronics, Microelectronics and Nanotechnology of Lille. After graduation in October 2020, his research is mainly focused on the development of SAW sensors and microsystems for fluids dynamics and aeronautics applications.

Romain Viard received his MS degree in Engineering with specialization in Micro-Nanotechnology, Wave Physics and Telecommunications from Ecole Centrale de Lille in 2006 and his PhD degree in 2010 from Ecole Centrale de Lille and the IEMN UMR CNRS 8520. During the research work presented in the paper he was at the Head of Innovation in Thurlemec Company in Pulversheim and CEO of Fluiditech. He joined in 2019 JMH Conception as R&D Engineer. His field of research concerns the development of innovative solutions for the manipulation and the measure of fluidic systems.

Eric Garnier is Dr, habilited, senior research engineer in the aerodynamics, aeroelasticity and acoustics department of ONERA. He is recognized as an expert in Large Eddy Simulation and flow control. He has contributed to 36 papers in peer-reviewed journals, 58 communications with proceedings and one textbook (LES for compressible flows with N. Adams and P. Sagaut). He has been involved in the supervision of 10 PhD Students and 8 master students.

Charles Poussot-Vassal is senior researcher with ONERA, the French aerospace lab (Toulouse, France). His research lies in the wide field of (mostly linear) dynamical model (rational) approximation, control design and analysis. A major part of his activities is dedicated to numerical developements and apply to a wide range of problems, including industrial-oriented applications.

Alain Merlen is Professor Emeritus at Lille University and a former chief scientist of the fluid mechanics and energetic branch at ONERA, The French national aerospace research centre, from 2012 to 2015. He is an expert for different French research evaluation agencies: French ministry of research, French agency of research (ANR), French agency of research evaluation (AERES), and

French national commission of universities (CNU). He is an expert for UE and UK Programs too. He supervised 23 PhDs, and he is author and co-author of 56 papers in peer review papers and 5 patents. He won 2 awards. He is a member of a NATO scientific Panel and a former Chaiman of the French academic society of mechanics (AUM).

Denis Sipp is Director of Research at ONERA, the French aerospace lab. He is the Scientific Officer of the Department of Aerodynamics, Aeroelasticity and Acoustics (DAAA). He obtained a PhD degree in 1999 on the stability of vortex pairs. His primary interest has moved to control of flow instabilities encountered in aeronautic applications, such as bluff bodies, cavities, boundary layers, jets, vortices or backward facing step flows. Both open-loop and closed-loop control strategies are considered with a special focus on linearized methods, adjoint techniques, model reduction, optimal control and numerical simulation.

Philippe Pernod received the Engineering Degree from Centrale Lille (1986), and the MS degree in ultrasound and imaging (1986), Ph.D. degree in Electronics (1989) and the Doctorat es-Sciences (1996) from University of Valenciennes. He is currently Full Professor at Centrale Lille, Head of the AIMAN-FILMS research group of Institute of Electronics, Microelectronics and Nanotechnology and Head on french side of the International Laboratory LICS in functional electronics, acoustics and fluidics. His research interests include nonlinear magnetoacoustics, Active multiferroic nanostructures, functional electronics, Micro-Magneto-Electro-Mechanical-Systems for sensors, actuators, microfluidics and RF devices, Nonlinear Ultrasonic imaging for the characterization of complex media and flows.

Abdelkrim Talbi is Professor at Centrale Lille and researcher at IEMN UMR CNRS 8520 Institute. He is a member of the International Laboratory on Critical and Supercritical phenomena in functional electronics, acoustics and fluidics (formerly LIA LICS- LEMAC). He received the MS degree in plasma, optics, electronics, and microsystems from the Universities of Metz, Nancy I, and Sup- Elec Metz, in 2000, and the PhD degree in 2003 (LPMIA) from the university of Nancy I. Researches of interest are invention, design, fabrication, characterization, and optimization of micro and nano electromechanical system (MEMS/NEMS): 1- micro-actuators (active materials), 2- micro-acoustic waves and resonant MEMS physical and bio sensors. 3- Micro-acoustic phononic crystals for sensors and microwaves applications. He has authored or coauthored of over 70 refereed publications and he is listed as co-inventor of 4 patents. He is IEEE Member and IEEE Sensor Member.

Authors statement

Thomas Arnoult : Conceptualization, Methodology, Validation, Formal analysis, Investigation, Writing - Original Draft, Writing - Review & Editing, Visualization ;

Colin Leclercq : Conceptualization, Methodology, Formal analysis, Writing - Review & Editing, Visualization, Supervision ;

Cécile Ghouila-Houri : Conceptualization, Methodology, Formal analysis, Writing - Review & Editing, Visualization, Supervision ;

Aurélien Mazzamurro : Conceptualization, Methodology, Formal analysis, Writing - Review & Editing, Visualization ;

Romain Viard : Writing - Review & Editing ;

Eric Garnier : Writing - Review & Editing ;

Charles Poussot-Vassal : Writing - Review & Editing ;

Alain Merlen : Writing - Review & Editing ;

Denis Sipp : Writing - Review & Editing, Visualization, Supervision ;

Philippe Pernod : Conceptualization, Methodology, Formal analysis, Writing - Review & Editing, Visualization, Supervision ;

Abdelkrim Talbi : Conceptualization, Methodology, Formal analysis, Writing - Review & Editing, Visualization, Supervision ;

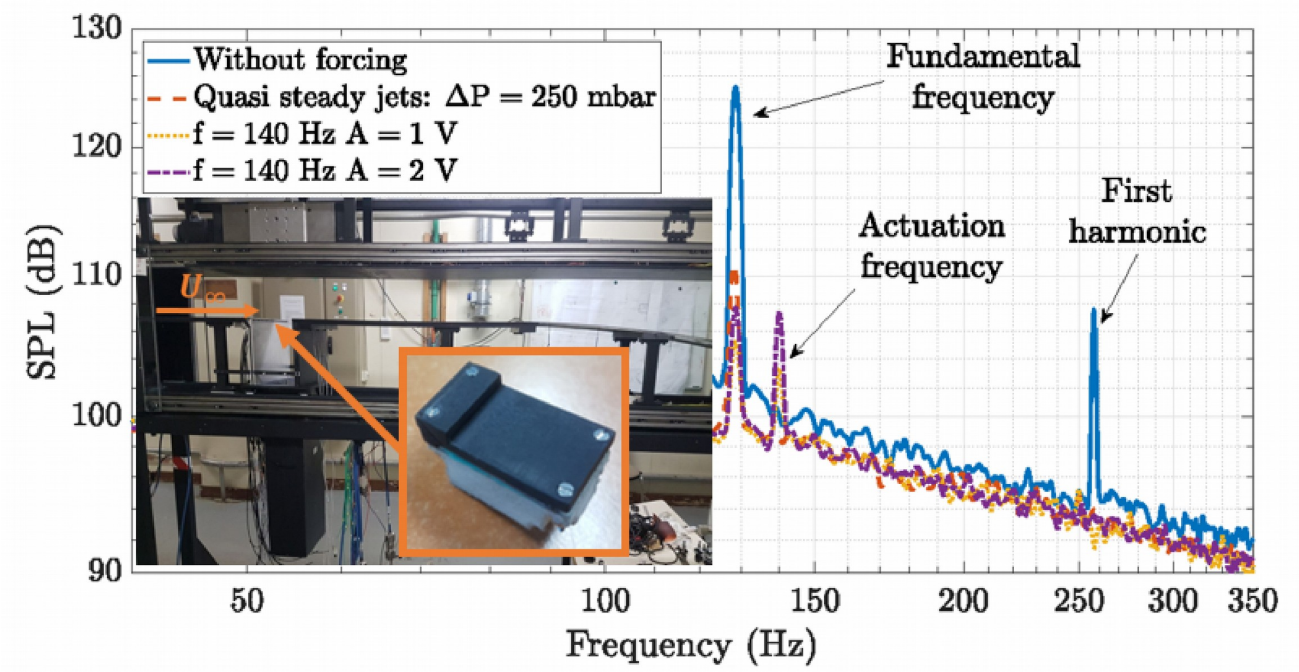
Without forcing
Quasi steady jets: ΔP = 250 mbar
f = 140 Hz A = 1 V
f = 140 Hz A = 2 V
Fundamental frequency
Actuation frequency
First harmonic
U_∞
SPL (dB)
Frequency (Hz)
130
120
110
100
90
50
100
150
200
250
300
350

Declaration of interests

☒ The authors declare that they have no known competing financial interests or personal relationships that could have appeared to influence the work reported in this paper.

☐ The authors declare the following financial interests/personal relationships which may be considered as potential competing interests: